Helical Carbon Nanotubes: Catalytic Particle Size-Dependent Growth and Magnetic Properties

Nujiang Tang,[†,*] Jianfeng Wen,[†] Yang Zhang,[†] Fanxin Liu,[†] Kuanjiuh Lin,[‡,*] and Youwei Du[†]

[†]Department of Physics and Nanjing National Laboratory of Microstructures, Nanjing University, Nanjing 210093, PR China, and [‡]Department of Chemistry and Center of Nanoscience and Nanotechnology, National Chung-Hsing University, Taichung 402, Taiwan, Republic of China

ABSTRACT The exact knowledge of helical carbon nanotube (HCNT) growth mechanism has not yet been completely clarified, and effective synthesis of high-purity helical carbon nanotubes in high yield still remains a tremendous challenge. In this study, HCNTs were synthesized *via* a catalytic chemical vapor deposition method using Fe nanoparticles as catalysts. We performed systematic experiments to investigate the specific effect of catalytic particle size (CPS) on the selective growth of HCNTs, such as on the morphology, yield, mobility of carbon atoms, and HCNT purity of carbon products. Our study showed that the CPS plays a key role in the selectivity to HCNTs, yield, and morphology of the carbon products, and a small catalytic particle is favorable to HCNT formation. We hope that this result may give a beneficial suggestion to obtain highly pure HCNTs. A CPS-dependent growth mechanism for HCNTs was finally proposed. Magnetic measurements demonstrated that the HCNTs are ferromagnetic properties and show high magnetization at room temperature.

KEYWORDS: carbon nanotubes · helical structures · catalytic growth · growth mechanism · magnetic property

HCNTs were first predicted to exist in the 1993 by Itoh *et al.*[1] and were first observed in 1994 by Zhang *et al.*[2,3] Thereafter, HCNTs have aroused continual and tremendous interest because of their helical structures, physical and chemical properties, and potential applications.[4−16] Generally, HCNTs can be produced as a byproduct in catalytic chemical vapor deposition (CCVD) of organic substances such as acetylene, pyridine, and toluene, using catalysts of transition metals at reaction temperatures ≥700 °C, with an inert carrier gas being used in most of the experiments.[17−19] To obtain high pure HCNTs, many researchers have performed detailed experiments to investigate the effects of specific synthesis parameters on the selectivity to HCNTs. For example, Piedigrosso *et al.*[20] reported that the presence of HCNTs was observed only in the sample with the lowest yield by lowest active Co−silica catalyst prepared by ion-adsorption precipitation at pH 9. They found that compared to the straight CNTs catalyzed by the other Co−silica catalyst prepared at higher pH value, the obtained HCNTs have the smallest diameter. Sarangi *et al.*[21] synthesized HCNTs which grew on Fe catalyst supported by kanthal wires by a cold-plasma CCVD route and investigated the effect of growth temperature on the HCNT growth. Their results showed that the increase in the growth temperature caused an increase in both the diameter and the coil pitch of the HCNTs. They suggested that it can be attributed to the decrease in number of the pentagon and heptagon pairs (P−H pairs) with increasing temperature. By applying a high bias to the wire, the number of spiral structures was reduced; instead, long aligned and self-supporting nanotubes were formed. Calles *et al.*[22] reported the HCNT growth on sulfonated Co−Mo/MgO sol−gel catalysts by CCVD thiophene vapor. Their studies demonstrated that the use of sulfur compounds during the sol−gel catalyst preparation process generally leads to a significant modification of the matrix composition and the matrix-catalyst interaction, resulting in the enhanced HCNT growth. However, sulfur introduced in the form of vapor over nonsulfonated catalysts leads to the enhanced growth of Y-shaped CNTs.

Moreover, HCNTs also can be synthesized as major products, and the effects of specific synthesis factors on the selective growth of HCNTs were discussed. For example, Hou *et al.*[23] reported the synthesis of HCNTs in large quantities by codecomposition of $Fe(CO)_5$ and pyridine or toluene at reaction temperatures ≥1000 °C under the flow of hydrogen. They studied the effect of decomposition temperature on the carbon morphology and found that, at the decomposition temperature of 700−800 °C, only carbon-coated Fe nanoparticles were obtained. Hernadi *et al.*[24] prepared HCNTs *via*

*Address correspondence to tangnujiang@nju.edu.cn, kjlin@dragon.nchu.edu.tw.

Received for review October 15, 2009 and accepted December 22, 2009.

Published online January 4, 2010.
10.1021/nn901425r

CCVD route using Co as catalyst and investigated the influence of catalytic preparation on HCNT growth by varying the pH of the solution during catalytic impregnation. Their experiments revealed that with increasing pH, $Co(OH)_2$ aggregates were larger in size. This resulted in the increase in both HCNT purity and average tube diameter of HCNTs, but resulted in the decrease of the yield. By CCVD method at 720 °C using Co nanoparticles supported on silica gel as catalysts under reduced pressure and at low gas flow rates, Lu *et al.*[25] fabricated dissimilar HCNTs. Very recently, a rational synthesis of HCNTs was reported by Rao *et al.*,[26] through the use of bimetallic In−Fe or Sn−Fe catalysts in a floating-catalyst-based CCVD at 700 °C. They performed experiments to elucidate the specific role of In and Sn catalysts, and proposed a model based on the mutual solubility of Fe with Sn and In and catalyst-growing nanostructure interactions. They found that In catalysts promote the growth of HCNTs while Sn-based catalysts catalyze the growth of helical carbon nanofibers (HCNFs) because of the relative affinity of Sn or In with the primary transition metal catalyst, Fe. Wang *et al.*[27] reported a novel method to obtain HCNTs at 850 °C using Cu as the catalyst and the periodical ethanol solution supply of the carbon source, where cupric acetate was dissolved in ethanol solution which was used as feeding. They investigated the effects of temperature and feeding flow rate on the selective growth of HCNTs and found that the feeding rate is a decisive factor to HCNT growth, and decomposition temperature can influence the HCNT structure. Their study showed that regular HCNTs can be grown only at a feeding rate of 30 mL/h and temperature of 850 °C. However, if the process is at a feeding rate of 50 mL/h, no HCNT can be found except for straight CNTs and Y-shaped CNTs. Moreover, besides by the conventional CCVD route, some other methods have been reported. For example, HCNTs also can be synthesized in the thermal reduction of ethyl ether over zinc in a stainless autoclave at 700 °C.[28] Moreover, a method for controlled synthesis of HCNTs was reported, in which aligned straight CNT arrays were used as a template.[29]

It is widely believed that the facet of the catalytic particle may lead to different extrusion velocities of carbon atoms, resulting in the HCNT growth. However, as mentioned above, these reports implied that only the facet is not enough to favor HCNT formation, *viz.*, it is not an exclusive factor. In fact, many synthesis factors play important roles in the selective HCNT growth. Recently, Szabó *et al.*[16] made a statistical analysis of the coil diameter distribution according to many reports, which showed that half of the coils are in the range of 50−70 nm, while again, half of the coils have a pitch in the range of 30−80 nm. They proposed that the geometric configuration of HCNTs is rather decided by the atomic structure of carbon layers building up the coils than by the synthesis factors which may induce the particular conditions favorable to coiling formation, and various synthesis factors may create the specific conditions to favor the selectivity to HCNT than to straight CNT. According to the experimental results reported by other researchers, we find that an important point which has been neglected is that compared to spring-like carbon microcoils, the tube diameter of most HCNTs is below 250 nm, close to that of catalytic particles they grow on. Notably, our previous work and many reports of other researchers frequently hinted that CPS does play a key role in the selective growth of HCNTs or HCNFs;[14,20,27,28,30−37] that is, there are some catalytic particles with relatively small size, which are favorable to the selective HCNT growth. Up to now, there still lacks systematic experiments to elucidate the specific effect of CPS on the selective growth of HCNTs, such as on the yield, morphology, and HCNT purity of carbon products. Therefore, it is worthwhile to investigate the correlation of the CPS and the selective HCNT growth.

In previous publications, we reported the synthesis of HCNFs[30] and HCNTs[31] in acetylene decomposition at a low temperature of 450 °C over Fe nanoparticles generated by means of a combined sol−gel/reduction method. We have investigated the effects of the catalyst amount adopted, the temperature for the introduction of acetylene, and the decomposition temperature on the selective growth of HCNFs and/or HCNTs in details. In the present study, we detected the effect of the CPS on the selective HCNT growth, and performed detailed experiments to elucidate the specific role of CPS. This would help to (i) see if there is a correlation between the CPS and selectivity to HCNTs; (ii) provide a reliable method to synthesize high-purity HCNTs in high yield, and give a fundamental suggestion to other researchers for the synthesis of highly pure HCNTs; and (iii) understand how and why the HCNTs are formed, and propose a HCNT growth mechanism. Moreover, due to the scientific interest and industrial applications of magnetic CNTs, the magnetic properties of the as-prepared and annealed HCNTs were also examined.

RESULTS AND DISCSSION

Figure 1 panels a−c show the TEM images of ferric oxide powders of no. 1, 2, and 3 catalytic precursors obtained by different amounts of raw materials, respectively. The images reveal that all of the catalytic precursor particles are not spherical but faceted. The size of no. 1, 2, and 3 particles are 15−30, 20−50, and 150−500 nm, respectively, confirming that the average size of particles increases with an increase of the raw material amount. As such, we can tailor the average size of catalytic precursor by changing the raw material amount. It is interesting to see that most of the particles are porous, which can be attributed to the combustion and decomposition of organometallic precursor and organism. One can see that the particles of

no. 1 and 2 exhibit good dispersion and have a relatively uniform grain size, while the size uniformity of no. 3 catalytic precursor particle is poor. Figure 1c shows that many particles of no. 3 catalytic precursor particles agglomerate in a big sheet which is even bigger than 1 μm. Shown in Figure 1d is a high magnification TEM image of Figure 1c, which demonstrates that there also exist some small catalytic precursor particles in no. 3 precursor sample, and big catalytic precursor particles are sheetlike.

Microstructures of Sample A. By using 163 mg of Fe_2O_3 nanoparticles as catalyst precursor, the yield of sample A is *ca.* 1.83 g in each run. Thus, high-yield HCNTs of *ca.* 1604% (the weight ratio of sample to Fe) were obtained by the CVD of acetylene at 475 °C. Figure 2a shows that the diameter of the tubes of the HCNTs is relatively uniform of *ca.* 100−200 nm; and the majority is 110 nm, which is similar to that reported previously.[22] As indicated by three white arrows in Figure 2b, three HCNTs which were ruptured by ultrasonic vibration shows the clear nozzles, indicating that the carbon helixes are HCNTs. Figure 2 panels a and b clearly show that two straight segments with the same length often symmetrically grow on two sides of a catalytic particle with a relatively big size of 120−200 nm. The content of HCNT with apparent straight segments and the diameter of 120−200 nm in sample A, as estimated by our systematic TEM and FE-SEM observations, is about 30%. However, almost no straight segments appear in the HCNTs grown on small catalytic particles with a diameter below 120 nm; and small HCNTs often are coiled in a regular and tight fashion, showing short pitches. An interesting phenomenon is that extensive FE-SEM and TEM investigations showed that the diameter and length of the straight segment increases with the increasing CPS. Namely, a big catalytic particle is useful to the growth of straight CNTs. As indicated by a white bidirectional arrow (shown in Figure 2b), a straight segment with the length up to *ca.* 1.6 μm grows over one side of the catalytic particle, indicating that a straight segment grew after the HCNT growth finished. This did not appear in the HCNFs or HCNTs grown on catalytic particles with small CPS reported previously.[30,31] We examined sample A by FE-SEM many times and estimated that the HCNT purity of sample A is *ca.* 85%, similar to that reported previously.[31]

It is known that graphite can be characterized by a Raman peak at 1580 cm^{-1} (called G-band), whereas the disorder in carbon materials would induce an intense "defect-induced" band at 1350 cm^{-1} (called D-band). Figure 2c shows the Raman spectra of the as-prepared sample A, and the red line is the superposition of the two fitted Gaussian−Lorentzian lines and the background/noise; the two green lines are the single fitted peaks. Two peaks appear at *ca.* 1345.3 and 1581.1 cm^{-1}, indicating the presence of disorder and/or distortion in the sample A. It is known that integrated Raman intensities I_D and I_G are proportional to the number of the scattering disordered and ordered sp^2 bonding carbon atoms in the illuminated area, respectively. The R of sample A is 1.4 according to the single fitted peaks. In other words, the existence of defects in the sample is highly likely.[29] The results illustrated that no. 1 catalyst can catalyze HCNTs with high HCNT purity and high yield at 475 °C.

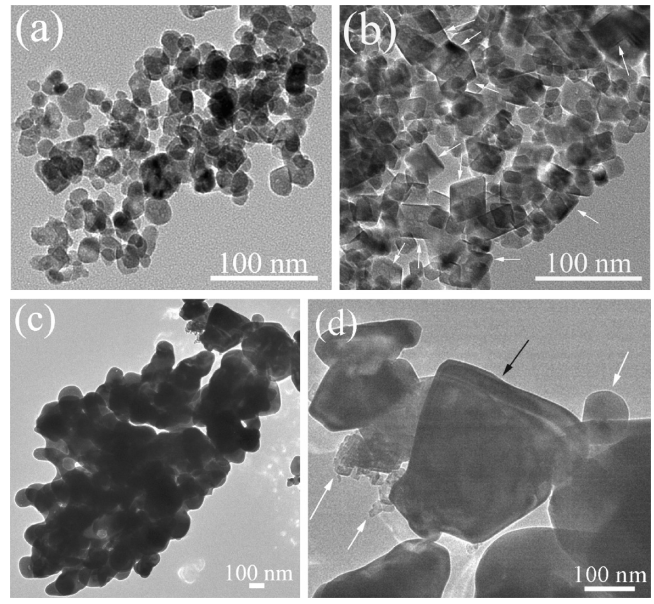

Figure 1. Transmission electron microscopy (TEM) images of catalytic precursors: ferric oxide particles of no. 1 (a), 2 (b), and 3 (c) catalytic precursors obtained by different amounts of raw materials; (d) high magnification image of panel c; the three white arrows indicate the small catalytic precursor particles, and the black arrow shows a big catalytic precursor sheet.

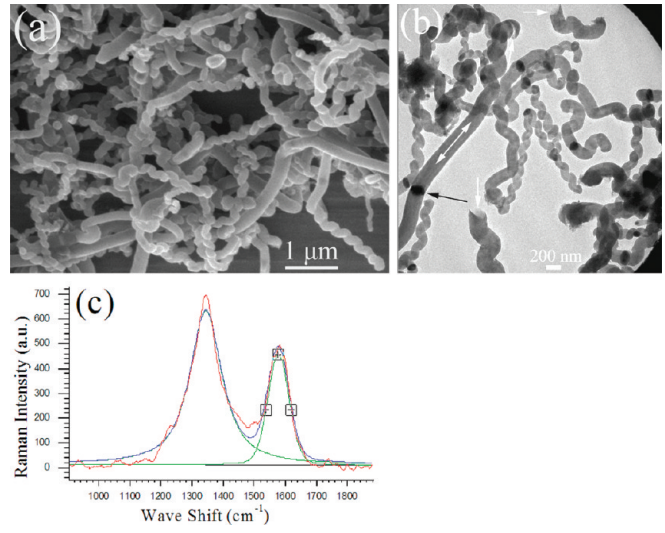

Figure 2. Microstructures of sample A: (a) field emission scanning electron microscopy (FE-SEM) image; (b) TEM image, the bidirectional arrow indicated a straight segment of a HCNT, and the white arrows indicate the nozzles of HCNTs; (c) Raman spectra. (The red line is the superposition of the two fitted Gaussian−Lorentzian lines and the background/noise; the two green lines are the single fitted peaks.)

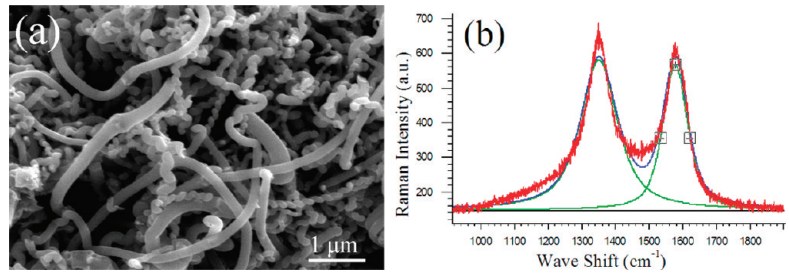

Figure 3. Microstructures of sample B catalyzed by no. 2 catalyst: (a) FE-SEM image; (b) Raman spectra. (The red line is the superposition of the two fitted Gaussian−Lorentzian lines and the background/noise; the two green lines are the single fitted peaks.)

Microstructures of Sample B. In contrast to the synthesis of sample A, a 5.318 g as-prepared sample B can be obtained in each run, demonstrating that no. 2 catalyst has better catalytic performance than no. 1 catalyst. Figure 3a shows the FE-SEM image of sample B. One can see that the HCNT purity (*ca.* 60%) is lower than that of sample A. An interesting phenomenon is that the morphology of the carbons is dependent on their size. Namely, only the small carbon products are HCNTs, while the large forms are straight CNTs. Apparently, the average diameter of the HCNTs is smaller than that of straight form. Such phenomenon also appeared in the growth of HCNTs using 328 mg of iron oxide as catalyst precursor, where carbon products with large diameter are of a straight form.[31] This also can be found in our previous work[30] and many reports of other researchers.[14,20,27,28,32−37] In the present investigation, by adopting the same type of Fe particles but with different size, one can generate varieties of yield and HCNT purity of carbon species at equal temperature. Therefore, one can deduce that the size of Fe particles has a determining effect on the yield and selectivity for HCNTs, and a small Fe particle is favorable to the growth of HCNTs with relatively low yield, whereas the big particle is useful to the growth of the straight form with high yield. Thus, we can obtain HCNTs with high HCNT purity at 475 °C by adopting small Fe nanoparticles. Figure 3b shows the Raman spectra of the as-prepared sample B, and the red line is the superposition of the two fitted Gaussian−Lorentzian lines and the background/noise; the two green lines are the single fitted peaks. It exhibits two peaks, one appears at *ca.* 1351.6 cm^{-1} (D-band) and the other appears at 1580.3 cm^{-1} (G-band), respectively. Compared to the G-band of the as-prepared sample A, the G-bands of sample B are down-shifted by *ca.* 0.8 cm^{-1}, denoting that there is a certain degree of rise in level of graphitization in sample B. Furthermore, the *R* of sample B is 1.04 according to the single fitted peaks, demonstrating further that the degree of graphitization of sample B is higher than that of sample A.

Microstructure of Sample C. We found that if no. 3 catalyst was used, the yield was *ca.* 3.481 g in each run, higher than that of sample A, but lower than that of sample B. Figure 4a shows a low magnification FE-SEM image of the as-prepared sample C, revealing that the HCNT purity is *ca.* 10% and the majority is CNT bundle. Moreover, one can find that the HCNTs have a small diameter and are always lone rather than showing HCNT bundle form. It is interesting to see that (i) a catalytic particle often locate at the node of two straight CNTs with almost the same diameter and length; (ii) in a CNT bundle, the size of the CNTs and/or the catalytic particles is relatively uniform, and the catalytic particles always locate at the same height of the bundle, showing a similar growth velocity. High-magnification FE-SEM and TEM images (Figure 4b,c) indicate that a big bundle often contains tens of small straight CNTs with relative uniform diameters of 100 nm. As shown in Figure 4c, two white arrows clearly indicate the nozzles of CNTs which were ruptured by ultrasonic vibration. Figure 4d shows sample C′ catalyzed by no. 3 catalyst for 20 min, revealing that there are many bundles which also contain some straight CNTs and are relatively uniform in the sample C′. It is interesting to find that (i) almost no catalytic particle wrapped in two straight CNTs is bigger than 150 nm in diameter in sample C; (ii) compared to the bundles in sample C, the bundles in sample C′ are shorter in the length and bigger in the diameter. Moreover, based on the fact that the catalytic particles may undergo grain growth and agglomeration during hydrogen reduction and acetylene decomposition, the catalytic particles (Fe particles) should be bigger than catalytic precursor particles. Apparently, a big catalytic sheet splits into tens of small catalytic particles during the growth of a CNT bundle, and tens of small straight CNTs align into a big bundle, which is similar to the result reported by Ning *et al.*[38]

CPS-Dependent Growth of HCNTs. On the basis of the results above, one can see an apparent phenomenon that the growth of carbon products is dependent on the CPS. As reported previously,[30,31] a HCNT or HCNF with good helical structure can grow on a catalytic particle with the *d* (diameter) $<$ 150 nm, whereas a HCNT with a straight segment extruded at the end of growth can grow on a catalytic particle with the *d* within the range of 150−200 nm, which is shown in sample A. If a catalytic sheet with the $d > 250$ nm was used, a CNT bundle can be obtained; this can be found in sample C. Therefore, the results showed that the CPS plays a key

role in the yield, HCNT purity, and selective growth of HCNTs, and one can obtain large-scale production of highly pure HCNTs by using small catalytic particles ($d < 150$ nm) as catalysts. Since well quantitative agreement is difficult due to the extremely complex conditions existing in the CVD reactor, our experimental data is approximately supported by our hypotheses.

Discussion of CPS-Dependent Growth Mechanism of HCNTs. To date, several mechanisms have been proposed for the HCNT growth. For example, Amelincks *et al.*[2] proposed a widely acceptable extrusion mismatch mechanism involving the mismatch between the extrusion velocities of carbon atoms from catalytic particle facet, which is favorable to HCNT growth. Similarly, based on the "anisotropy of carbon deposition" theory, Motojima *et al.*[42] provided a new growth mechanism for amorphous carbon coils. This relies on an assumption that the symmetric catalytic activities on six crystallographic facets determine the formation of carbon coils. Dunlap[39,40] suggested a heptagon−pentagon (H−P) construction mechanism to explain the formation of graphite HCNTs, which involved the periodic introduction of the H−P pairs into Hx (hexagon) network during the CNT growth. On the basis of the H−P construction, Gao *et al.*[19] and Lu *et al.*[25] proposed a HCNT mechanism, which involves graphite core formation centering on a catalytic particle followed by graphite HCNT growth. Also on the basis of the H−P construction mechanism, Terrones *et al.*[41] made a modification and suggested that high mobility of carbon atoms can easily quench *n*-Hx (H or P) rings in the growing nucleus, resulting in graphite layers with perfect Hx network and forming straight CNTs. In contrast, low mobility of carbon atoms is favorable to the formation of *n*-Hx rings and growth of HCNTs. Thereafter, Birǒ *et al.*[8] reinforced further the modified mechanism, and suggested that a fast kinetic leading to metastable states that cannot anneal out at low growth temperature contributes to the HCNT growth. However, it is worthwhile to note that the H−P construction mechanism is effective in explaining the growth of graphite HCNTs, rather than the formation of amorphous carbon coils.[34−37,42]

Combined with the character of the faceted catalytic particle, it should be trustworthy that the asymmetric velocity in carbon extrusion resulting from the facet as proposed by Amelincks *et al.*[2] contributes to the formation of HCNTs. However, it is notable that the same type faceted Fe nanoparticles were used as catalysts, but one can find that the CPS (also including other synthesis conditions, such as amount of catalyst adopted, and decomposition temperature, *etc.*) has a profound influence in selective HCNT growth according to our present and previous investigations.[30,31] For example, by adopting no. 1 catalyst with small CPS, one can generate sample A with high HCNT purity at 475 °C. However, by adopting no. 3 catalyst with big CPS, one can obtain sample C with low HCNT purity at equal

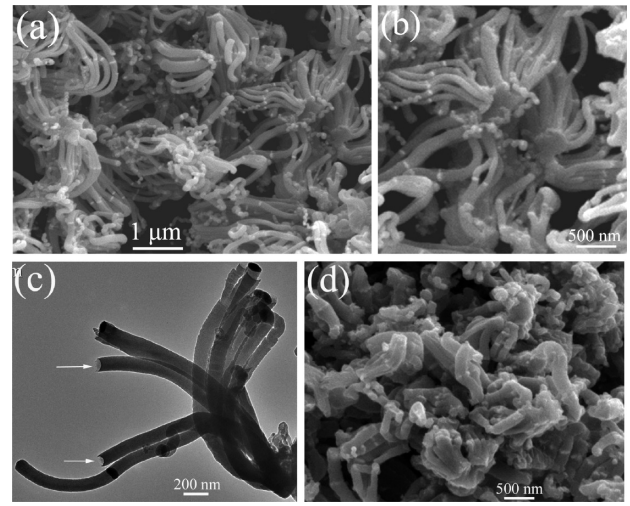

Figure 4. Microstructures of sample C catalyzed by no. 3 catalyst: (a) low-magnification FE-SEM image; (b) a high-magnification FE-SEM image of a typical bundle; (c) TEM image, and two white arrows indicate the nozzles of CNTs which were ruptured by sonic dispersion; (d) FE-SEM image of sample C′ catalyzed by no. 3 catalyst for 20 min.

temperature. Moreover, a straight part can be extruded at the end of the HCNT growth in the cases of samples A and B, but not appear in the cases of HCNFs and HCNTs catalyzed by smaller catalysts.[30,31] Apparently, the continuous existence of the facet on the surface of catalytic particle and the facet effect during all the growth period is another necessary factor for the selective HCNT growth. However, there often is a deformation in the catalytic particle during the acetylene decomposition, resulting in the decreasing in the curvature of the facet and in the facet effect during the successive decomposing period. Therefore, it is necessary to modify the mechanism proposed by Amelincks *et al.*,[2] and the new growth mechanism should be catalytic particle size-dependent and involve the catalytic particle deformation during the acetylene decomposition.

To discuss the size-dependent growth mechanism and the deformation in the catalytic particle, it is necessary to investigate the initial shape before the acetylene decomposition and *in situ* deformation of the catalytic particle during the acetylene decomposition, and then analyze the facet effect. However, because of the poor air stability of nanoscaled iron, the *in situ* investigations of the initial shape and deformation of Fe nanoparticles during the acetylene decomposition are difficult. Thus, it is feasible to obtain a midshape before the final shape after deformation and study the difference of the midshape and final shape of catalytic particle. By decreasing the time of acetylene decomposition from 1 h to 20 min, we synthesized sample A′ *via* the same fabrication process of sample A. The result shows that there is a great decreasing in the yield (*ca.* 1.311 g in each run). Figure 5 panels a and b show that sample A′ is shorter than sample A, but similar in diameter and

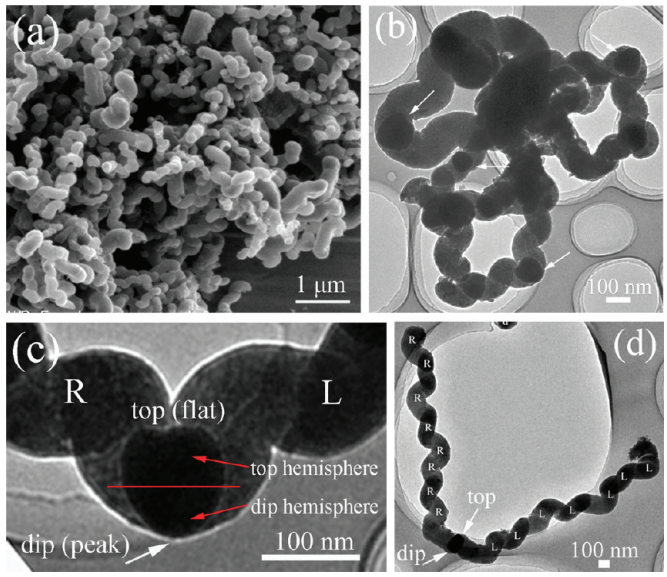

Figure 5. Microstructure of the sample A′ obtained using no. 1 catalyst: (a) FE-SEM image; (b) TEM image. The arrows indicate the cordate catalytic nanoparticles located at twinned HCNTs. (c) Magnified image of the node at which catalytic particle is located in panel b; right-handed HCNT indicated by "R" and left-handed HCNT indicated by "L"; the "top" and "dip" direct the flat part and peak part of the cordate catalytic particle, respectively. (d) A typical TEM image of a catalytic nanoparticle wrapped at the node between two HCNTs of sample A.

HCNT purity. Shown in Figure 5c is a typical catalytic particle with cordate shape wrapped in the node of two HCNTs. This reveals that the carbon layer thickness on peak and flat sites of the particle always is much thinner than on other sites of the particle, demonstrating that the peak and flat sites are low extrusion sites of carbon atoms, while other sites are high extrusion sites. Namely, the peak and flat sites of the cordate particle are the absorbing and decomposing points of acetylene[23] but are low extrusion sites of carbon atoms, while other sites prematurely lose their catalytic activation and are the high extrusion sites. Moreover, according to the curling direction (shown in Figure 5c), it is reasonable to estimate that there is an increasing extrusion tendency from peak to flat part on the surface of catalytic particle. The consequence is that the extrusion velocity of carbon atoms on the top hemisphere of the cordate particle is higher than on the dip hemisphere. Thus, this will result in mismatch extrusion of carbon atoms between the dip and top hemispheres of the cordate particle surface, favorable to the formation of HCNTs. It is similar to the facet effect,[2] and herein is peak effect. This also can be observed in our previous work.[30,31]

If two cordate catalytic particles have different size, and each of them has a peak with same size, we can make an assumption that the two peaks have an equal low extrusion of carbon atoms. In the dip hemisphere, because the small catalytic particle has fewer nonpeak sites than the big catalytic particle, it is reasonable to conclude that the small catalytic particle has a higher ratio of peak site *versus* nonpeak site, or say, higher ratio of low extrusion site *versus* high extrusion site than the big one. Apparently, two conclusions can be made: (i) the degree of extrusion mismatch on the dip and top hemispheres in small catalytic particle is higher than that in the big one. Namely, the degree of carbon atoms asymmetric extrusion in small catalytic particles will be more drastic than that in the big one. Or say, the facet effect should be more effective in small catalytic particles than in big ones. Therefore, the selectivity to HCNTs on small catalytic particles is higher than that on the big ones. (ii) The extrusion velocity of carbon atoms in small catalytic particles should be lower than big ones. As a result, the rate of acetylene decomposition on small catalytic particles will be lower than that on big ones. Thus, the HCNT purities of samples A and A′ are higher than that of samples B and C. However, the yields of samples A and A′ are lower than that of samples B and C, as shown in Table 1.

Notable, acetylene decomposition is an exothermic reaction. Thus, the temperature of catalytic particle will increase during the acetylene decomposition on its surface, and is dependent of the rate of acetylene decomposition. Therefore, the high extrusion of carbon atoms in big catalytic particles may enhance the rate of acetylene decomposition on its surface. This will result in the increase in its temperature and can enhance its catalytic activity further. Apparently, big catalytic particles will have higher temperature than small ones. As we know that the nanoscaled particle is metastable at high temperature, which may cause the catalytic particle to undergo the deformation from initial faceted particle with a large curvature to a cordate one with decreased curvature, and lastly to the one with a small curvature or with a flat surface. A consequence is that the facet effect will disappear early in a big catalytic particle, which favors the selective growth of straight form. This may be the reason that a straight part often is extruded at the end of the HCNT growth in the case of using no. 2 catalyst, while straight CNTs is the main form in the case using no. 3 catalysts. Or say, the facet effect prematurely disappeared and the asymmetry in carbon atoms extrusion on big catalytic particle was lowered further because of the deformation involving the decreasing in the curvature of the peak part, which resulted from increasing temperatures in the cases of the samples B and C. It also can be confirmed that HCNTs always are small and lone rather than big or forming CNT bundles in sample C.

As shown in Figure 5d, one can find that the curvature of the dip part of sample A is smaller that that of peak part of sample A′ (shown in Figure 5c), demonstrating that there is a decrease in the curvature in the catalytic particle. Or say, there is a deformation from cordate shape to flat shape in the peak part of small catalytic particle. Namely, there will be a deformation in the catalytic particle during the HCNT growth, which is attributed to the temperature increasing because of

TABLE 1. The Dependence of CPS on the Selective HCNT Growth

sample	catalyst (no.)	average size of catalytic precursor particle	yield (g)	rate of C_2H_2 decomposition	temperature of catalytic particle	HCNT purity (%)	facet effect
A	1	small	1.83	low	low	85	strong
B	2	big	4.732	highest	highest	60	weak
C	3	biggest	3.481	high	high	10	weakest

the acetylene decomposition. Notable, this can be achieved *via* increasing the catalyst amount adopted[31] or increasing the initial decomposition temperature,[30] or vice versa. For example, in the case of sample A′, the decreasing in the rate of acetylene decomposition because of the decreasing in the catalyst amount adopted resulted in the decreasing in thermal release during acetylene decomposition. Therefore, the increasing in the catalytic particle temperature of sample A′ during acetylene decomposition will be slower and slighter than that of sample A. As a result, the deformation of the catalytic particle of sample A′ is also slighter than that of sample A. Since there is a deformation from cordate shape to the *n*-cordate one in the catalytic particle of sample A, the peak effect will be lowered during the acetylene decomposition. This may be the reason that compared to sample A, almost no straight segment appeared in sample A′, small HCNFs,[30] or HCNTs[31] reported previously; while a longer straight segment will be extruded on a bigger catalytic particle at the end of the growing period (as shown in Figures 2a,b). It is reasonable to conclude that (i) the catalytic particle shape of sample A′ is more close to the initial shape of no. 1 catalyst than that of sample A; (ii) there is a deformation from the initial shape to cordate shape and last to the *n*-cordate one with smaller curvature.

According to above analysis, a small catalytic particle with facet is the primary and starting factor to the selective HCNT formation in this size-dependent growth mechanism. However, the continuous existence of the facet and the facet effect during all the growth period is another necessary factor for the selective HCNT growth. There apparently exists a CPS effect in the efficiency of facet effect because the facet effect will be diluted with the increasing in the CPS. Furthermore, the temperature of big catalytic particles may increase fast and should remain high because of the drastic and continuous exothermic reaction, which can enhance the decomposition of acetylene and extrusion of carbon atoms. Thus, the curvature of big catalytic particle may decrease fast, resulting in decreasing the curvature of the facet, and lowering the asymmetry in extrusion further.

Shown in Figure 6 is a TEM image of sample C′ catalyzed by no. 3 catalyst for 20 min. One can find an interesting phenomenon that the catalytic particles located at the nodes of small straight CNTs in sample C′ have similar CPS of no. 1 catalyst and also are faceted. However, the carbon products are straight form rather than HCNTs. Therefore, a facet effect only is not effective enough to represent the selective HCNT growth. We consider that the low mobility of carbon atoms should be another important factor to the selective HCNT formation, which agrees with the H−P construction mechanism proposed by Terrones *et al*,[41] namely, asymmetric extrusion velocity of carbon atoms resulting from facet effect is a key factor for the selective HCNT growth, and the low mobility of carbon atoms is another necessary factor. Therefore, it is worth discussing the two mechanisms of the extrusion mismatch mechanism and H−P construction mechanism.

It is well-known that incorporation of *n*-Hx into the Hx network can induce curvature into the graphite tube, and continuous extrusion of a carbon *n*-Hx-inserted Hx network would result in the formation of HCNTs.[23,41] Thus, low mobility of carbon atoms throughout acetylene decomposition is another key factor for the selective HCNT growth. Because the small catalytic particle has a low rate of acetylene decomposition and maintains relatively low temperature, the mobility of carbon atoms can keep relatively low and stable. Apparently, this can contribute the successive selectivity to HCNTs. For example, in the cases of samples A and A′ catalyzed by no. 1 catalyst, both the temperature of catalytic particle and the rate of acetylene decomposition keep relatively low, resulting in low mobility of carbon atoms. As a result, *n*-Hx rings can be quenched in the HCNT growth; that is, the glide of *n*-Hx rings may be avoided by adopting no. 1 small catalyst.[41] On the contrary, in the cases of no. 2 and 3 big catalytic particles, the mobility of carbon atoms is high and will make *n*-Hx rings glide easily and will contribute well to the Hx network. As shown in samples B, the average diameter of the straight CNTs is larger than that of the HCNTs; the consequence is poor selectivity to HCNTs. The result is consistent with the statistical result reported by Szabó *et al*.,[16] and also confirmed by the Raman results is that the level of graphitization of sample B is higher than that of sample A. As to the cases of samples C and C′, because the CPS of no. 3 catalytic particle is big and the temperature of the catalytic particle is high, the mobility of carbon atoms is also high. Thus, it is reasonable to conclude that (i) the facet effect is a primary and starting factor to the initial selective growth of HCNTs; (ii) the small CPS, which favors maintaining a low temperature of catalytic particle and low

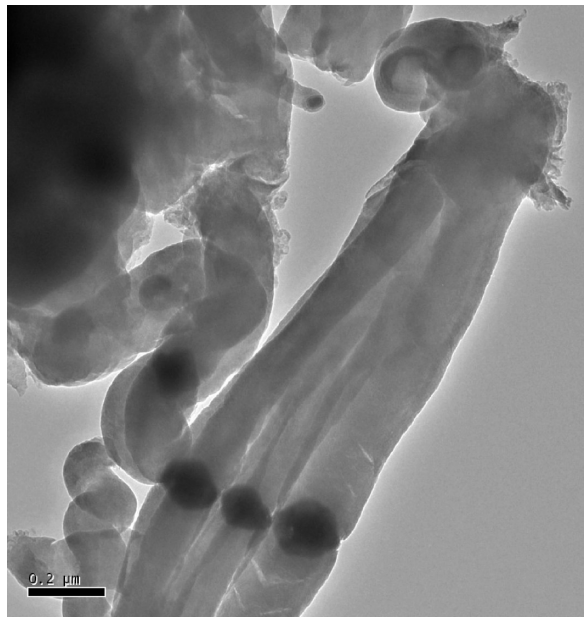

Figure 6. TEM image of sample C′ catalyzed by no. 3 catalyst for 20 min.

mobility of carbon atoms, is the other necessary factor of the successive growth of HCNTs; (iii) the two factors of CPS and catalytic particle temperature coexist and interrelate in the growth of carbon products.

As shown in Table 1, our study reveals that (i) the CPS has a profound influence in the selective HCNT growth, such as in the yield, rate of acetylene decomposition, temperature of catalytic particle, mobility of carbon atoms, and HCNT purity; (ii) with the increase in CPS, the facet effect will lower. Thus, to obtain highly pure HCNTs, the fabrication of uniform and small catalytic particles is a key process. Moreover, this mechanism is clear in the present experiment and also effective to other reports.[43] Therefore, it is reasonable to deem that the new size-dependent growth mechanism which mixes the two mechanisms is more reliable and comprehensive than either of the two mechanisms to elucidate the selective HCNT growth.

Magnetic Properties of the as-Prepared and Annealed Samples A and A′. Recently, magnetic CNTs have aroused much attention because they have applications in wearable electronics, cantilever tips in magnetic force microscopes, magnetic stirrers in microfluidic devices, magnetic valves in nanofluidic devices and magnetic inks, drug delivery, magnetic resonance imaging, *etc.*[44] However, the applications of CNTs in magnetism are still limited because of their low magnetization. To enhance magnetization and realize the applications of CNTs in magnetism, it is necessary to increase the content of magnetic particle. Thus, researchers often introduce foreign magnetic particles by filling them inside hollow cavities or coating them on the outer surfaces of CNTs. For example, Jang *et al.*[45] filled CNTs with γ-Fe_2O_3 *via* a metal-impregnated polymer precursor, and the M_S of the CNTs composites reached up to *ca.* 7.1 emu/g. Xu *et al.*[46] encapsulated CNTs with Fe_3O_4 nanowires by pyrolyzing an ethanol/ferrocene mixture in an autoclave at 600 °C, and the M_S of the CNTs composites is *ca.* 5.11 emu/g. Figure 7a shows the $M-H$ curves of the as-prepared sample A and the annealed sample A. One can find that the M_S and the H_c of the as-prepared sample A are high, up to 7.47 emu/g and 266.21 Oe, respectively. We estimate that the amount of Fe_3C presence was *ca.* 6.68 wt %. On the basis of the Fe_3C content and the magnetization of Fe_3C, we estimate a M_S of 8.55 emu/g, higher than the experimental value of 7.47 emu/g. This can be related to the nonuniformity in magnetic properties of as-prepared HCNTs due to the uneven distribution of Fe_3C nanoparticles in the composite sample. In an attempt to enhance the M_S of HCNTs, we annealed the sample in Ar at 750 °C for 4 h. We reported previously that there is a transformation of Fe_3C to α-Fe and C during the annealing procedure.[31] Figure 6a also shows the $M-H$ curve of the annealed sample A. The M_S of the annealed sample increased to 12.77 emu/g, while its H_c decreased to 168.94 Oe. Since α-Fe is the major phase in the annealed sample, we consider that the amount of α-Fe presence is about *ca.* 6.24 wt %. On the basis of the Fe content and the facts that the magnetization of α-Fe is *ca.* 220 emu/g at 300 K, we estimate that the M_S of the annealed sample should be *ca.* 13.73 emu/g, which is higher than the 12.77 emu/g value obtained experimentally. Compared to the as-prepared sample, the annealed samples with encapsulated α-Fe nanoparticles are higher in magnetization.

Figure 7b shows the $M-H$ curve of the as-prepared and annealed samples A′. The M_s and the H_c of the as-prepared sample A′ are 11.08 emu/g and 137.04 Oe, respectively. We estimate that the amount of Fe_3C present was *ca.* 8.75 wt %. We estimate an M_s of 11.2 emu/g, a little higher than the experimental value of 11.08 emu/g. Compared to the as-prepared sample A, the as-prepared sample A′ is much higher in magnetization because of its higher amount of Fe_3C presence. A higher M_S and a lower H_c of 17.86 emu/g and *ca.* 100 Oe, respectively, can be obtained in the annealed sample. Compared to the CNTs reported, our HCNTs have higher magnetization. Moreover, their magnetization can be enhanced by decreasing the amount of catalyst and/or annealing them at high temperature.

CONCLUSIONS

In conclusion, we have illustrated how the yield and HCNT purity of the HCNTs can be manipulated *via* changing the size of catalytic particles. We also have detected the effect of the CPS on the selective growth of HCNTs and performed detailed experiments to elucidate the specific role of CPS in the selective growth of HCNTs. Our study demonstrates that a small catalytic particle with facet or peak is the primary and starting factor to the selective HCNT formation in this mixed

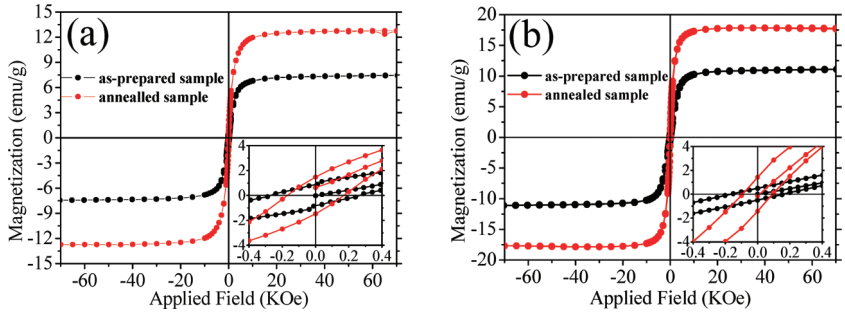

Figure 7. Typical magnetization curves of the as-prepared and annealed samples measured at 300 K by SQUID; the maximum applied field was 7 kOe: (a) sample A, and (b) sample A′. Insets are the parts of the corresponding magnetization curves.

mechanism, and the continuous existence of facet on the catalytic particle throughout the growth period is another necessary factor for the selective HCNT growth. Moreover, a small catalytic particle is favorable to low mobility of carbon atoms, and thus the HCNT formation. The new size-dependent growth mechanism combining facet effect and mobility of carbon atoms is reasonable and effective to selective HCNT growth. We hope that understanding this new growth mechanism will help in obtaining highly pure HCNTs *via* small catalytic particles. Magnetic measurements reveal that the HCNTs display ferromagnetic properties with relatively high magnetization at room temperature (rt) and have appealing applications.

EXPERIMENTAL SECTION

Experimental Procedure. The objective of the present work is to investigate the effect of CPS on the selective HCNT growth. To this end, the amount of raw materials was changed to prepare the catalytic precursors with different size. In this work, $FeCl_2 \cdot 4H_2O$, citric acid monohydrate and ethanol absolute were used as the raw material, coordination agent, and solvent, respectively. To prepare no. 1, 2, and 3 catalyst precursors with different size, the amounts of $FeCl_2 \cdot 4H_2O$ and citric acid monohydrate were 0.01 and 0.015 mol, 0.03 and 0.045 mol, 0.05 and 0.075 mol, respectively. In a typical experiment, $FeCl_2 \cdot 4H_2O$ and citric acid monohydrate were dissolved in 100 mL of ethanol absolute and stirred at 60 °C for 6 h. After being dried at 80 °C, the xerogel was heated at 450 °C for 3 h in air and turned into ferric oxide. No. 1, 2, and 3 catalytic precursors were used for the synthesis of samples A, B, and C, respectively. For the generation of the samples adopted in the present study, we used a similar approach reported previously, namely, 163 mg of catalytic precursor powder was spread on a ceramic plate which was placed in a quartz reaction tube (5 cm inner diameter and 35 cm in length). This assembly was laid in a stainless steel reaction tube of 5.2 cm inner diameter and 80 cm in length (equipped with temperature and gas-flow controls). Therefore, the iron oxide was reduced in H_2 at 425 °C for 4 h, and the acetylene decomposition was conducted at 475 °C for 1 h at atmospheric pressure over the Fe catalyst. After the system was cooled to rt, the as-prepared sample was obtained.

Characterization of the Samples. Raman spectroscopic investigation of the samples was performed using a Jobin-Yvon LABRAM HR800 instrument with 514.5 nm Ar laser excitation. The morphologies of the samples were examined by TEM (model JEM-2100, Japan), and FE-SEM (model JSM-6700F, Japan) with the equipment operated at an accelerating voltage of 200, and 5 kV, respectively. For TEM analysis, the powder samples were dispersed in ethanol, agitated in an ultrasonic bath, and finally deposited on a copper grid that was coated with a carbon film. The magnetic properties of samples were measured at rt by a SQUID magnetometer (Quantum Design MPMS-XL, USA) equipped with a superconducting magnet capable of producing fields of up to 70 kOe.

Acknowledgment. This work was financially supported by the Jiangsu Provincial Natural Science Foundation for Young Innovator (BK2007522), and the National Major Projects of Fundamental Research (2005CB623605 and 2010CB923402) P. R. China, and the National Science Council of Taiwan (NSC96-2627-M-005-001).

REFERENCES AND NOTES

1. Itoh, S.; Ihara, S.; Kitakami, J. Toroidal Form of Carbon C_{360}. *Phys. Rev. B* **1993**, *47*, 1703–1704.
2. Amelinckx, S.; Zhang, X. B.; Bernaerts, D.; Zhang, X. F.; Ivanov, V.; Nagy, J. B. A Formation Mechanism for Catalytically Grown Helix-Shaped Graphite Nanotubes. *Science* **1994**, *265*, 635–639.
3. Zhang, X. B.; Zhang, X. F.; Bernaerts, D.; Van Tendeloo, G.; Amelinckx, S.; Landuyt, J. V.; Vanov, V.; Nagy, J. B.; Lambin, P.; Lucas, A. A. The Texture of Catalytically Grown Coil-Shaped Carbon Nanotubules. *Euro. Phys. Lett.* **1994**, *27*, 141–146.
4. Iijima, S.; Toshinary, I.; Ando, Y. Pentagons, Heptagons and Negative Curvature in Graphite Microtubule Growth. *Nature* **1992**, *356*, 776–778.
5. Ihara, S.; Itoh, S. Helically Coiled and Toroidal Cage Forms of Graphitic Carbon. *Carbon* **1995**, *33*, 931–939.
6. Akagi, K.; Tamura, R.; Tsukada, M.; Itoh, S.; Ihara, S. Electronic Structure of Helically Coiled Cage of Graphitic Carbon. *Phys. Rev. Lett.* **1995**, *74*, 2307–2310.
7. Zhong, O. Y.; Su, Z. B.; Wang, C. L. Coil Formation in Multishell Carbon Nanotubes: Competition between Curvature Elasticity and Interlayer Adhesion. *Phys. Rev. Lett.* **1997**, *78*, 4055–4058.
8. Birü, L. P.; MÜrk, G. I.; Koüs, A. A.; Nagy, J. B.; Lambin, P. Coiled Carbon Nanotube Structures with Supraunitary Nonhexagonal to Hexagonal Ring Ratio. *Phys. Rev. B* **2002**, *66*, 165405.
9. Akagi, K.; Tamura, R.; Tsukada, M.; Itoh, S.; Ihara, S. Electronic Structure of Helically Coiled Carbon Nanotubes: Relation Between the Phason Lines and Energy Band Features. *Phys. Rev. B* **1996**, *53*, 2114–20.
10. Volodin, A.; Ahlskog, M.; Seynaeve, E.; Haesendonck, C. Van; Fonseca, A.; Nagy, J. B. Imaging the Elastic Properties of Coiled Carbon Nanotubes with Atomic Force Microscopy. *Phys. Rev. Lett.* **2000**, *84*, 3342–3345.
11. Fonseca, A. F.; da; Galvão, D. S. Mechanical Properties of Nanosprings. *Phys. Rev. Lett.* **2004**, *92*, 175502.
12. Chen, X. Q.; Zhang, S. L.; Dikin, D. A.; Ding, W. Q.; Ruoff, R. S.; Pan, L. J.; Nakayama, Y. Mechanics of a Carbon Nanocoil. *Nano Lett.* **2003**, *3*, 1299–1304.

13. Bajpai, V.; Dai, L. M.; Ohashi, T. Large-Scale Synthesis of Perpendicularly Aligned Helical Carbon Nanotubes. *J. Am. Chem. Soc.* **2004**, *126*, 5070–5071.
14. Xie, J. N.; Mukhopadyay, K.; Yadev, J.; Varadan, V. K. Catalytic Chemical Vapor Deposition Synthesis and Electron Microscopy Observation of Coiled Carbon Nanotubes. *Smart Mater. Struct.* **2003**, *12*, 744–748.
15. Volodin, A.; Buntinx, D.; Ahlskog, M.; Fonseca, A.; Nagy, J. B.; Van Haesendonck, C. Coiled Carbon Nanotubes as Self-Sensing Mechanical Resonators. *Nano Lett.* **2004**, *4*, 1775–1779.
16. Szabü, A.; Fonseca, A.; Nagy, J. B.; Lambin, P.; Birü, L. P. Structural Origin of Coiling in Coiled Carbon Nanotubes. *Carbon* **2005**, *43*, 1628–1633.
17. Cheng, J. P.; Zhang, X. B.; Tu, J. P.; Tao, X. Y.; Ye, Y.; Liu, F. Catalytic Chemical Vapor Deposition Synthesis of Helical Carbon Nanotubes in Triple Helices Carbon Nanostructure. *Mater. Chem. Phys.* **2006**, *95*, 12–15.
18. Ivanov, V.; Fonseca, A.; Nagy, J. B.; Lucas, A.; Lambin, P.; Bernaerts, D.; Zhang, X. B. Catalytic Production and Purification of Nanotubules Having Fullerene-Scale Diameters. *Carbon* **1995**, *33*, 1727–1738.
19. Gao, R. P.; Wang, Z. L.; Fan, S. S. Kinetically Controlled Growth of Helical and Zigzag Shapes of Carbon Nanotubes. *J. Phys. Chem. B* **2000**, *104*, 1227–1234.
20. Piedigrosso, P.; Konya, Z.; Colomer, J. F.; Fonseca, A.; Tendeloo, G. V.; Nagy, J. B. Production of Differently Shaped Multiwall Carbon Nanotubes Using Various Cobalt Supported Catalysts. *Phys. Chem. Chem. Phys.* **2000**, *2*, 163–170.
21. Sarangi, D.; Karimi, A. Bias-Enhanced Growth of Carbon Nanotubes Directly on Metallic Wires. *Nanotechnology* **2003**, *14*, 109–112.
22. Valles, C.; Perez-Mendoza, M.; Castell, P.; Martinez, M. T.; Maser, W. K.; Benito, A. M. Towards Helical and Y-Shaped Carbon Nanotubes: The Role of Sulfur in CVD Processes. *Nanotechnology* **2006**, *17*, 4292–4299.
23. Hou, H. Q.; Jun, Z.; Weller, F.; Greiner, A. Large-Scale Synthesis and Characterization of Helically Coiled Carbon Nanotubes by Use of $Fe(CO)_5$ as Floating Catalyst Precursor. *Chem. Mater.* **2003**, *15*, 3170–3175.
24. Hernadi, K.; Thien-Nga, L.; Forro, L. Growth and Microstructure of Catalytically Produced Coiled Carbon Nanotubes. *J. Phys. Chem. B* **2001**, *105*, 12464–12468.
25. Lu, M.; Li, H. L.; Lau, K. T. Formation and Growth Mechanism of Dissimilar Coiled Carbon Nanotubes by Reduced-Pressure Catalytic Chemical Vapor Deposition. *J. Phys. Chem. B* **2004**, *108*, 6186–6192.
26. Wang, W.; Yang, K. Q.; Gaillard, J.; Bandaru, P. R.; Rao, A. M. Rational Synthesis of Helically Coiled Carbon Nanowires and Nanotubes through the Use of Tin and Indium Catalysts. *Adv. Mater.* **2008**, *20*, 179–182.
27. Wang, J. N.; Su, L. F.; Wu, Z. P. Growth of Highly Compressed and Regular Coiled Carbon Nanotubes by a Spray-Decomposition Method. *Cryst. Growth Des.* **2008**, *8*, 1741–1747.
28. Luo, T.; Liu, J. W.; Chen, L. Y.; Zeng, S. Y.; Qian, Y. T. Synthesis of Helically Coiled Carbon Nanotubes by Reducing Ethyl Ether with Metallic Zinc. *Carbon* **2005**, *43*, 755–759.
29. Zhang, G. Y.; Liu, S.; Wang, E. G. Patterned Growth of Coiled Carbon Nanotubes by a Template-Assisted Technique. *Appl. Phys. Lett.* **2004**, *84*, 2646–2648.
30. Tang, N. J.; Zhong, W.; Gedanken, A.; Du, Y. W. High Magnetization Helical Carbon Nanofibers Produced by Nanoparticle Catalysis. *J. Phys. Chem. B* **2006**, *110*, 11772–11774.
31. Tang, N. J.; Zhong, W.; Au, C. T.; Gedanken, A.; Yang, Y.; Du, Y. W. Large-Scale Synthesis, Annealing, Purification, and Magnetic Properties of Crystalline Helical Carbon Nanotubes with Symmetrical Structures. *Adv. Funct. Mater.* **2007**, *17*, 1542–1550.
32. Tang, N. J.; Yang, Y.; Lin, K. J.; Zhong, W.; Au, C. T.; Du, Y. W. Synthesis of Plait-like Carbon Nanocoils in Ultrahigh Yield, and Their Microwave Absorption Properties. *J. Phys. Chem. C* **2008**, *112*, 10061–10067.
33. Tang, N. J.; Zhong, W.; Au, C. T.; Yang, Y.; Han, M. G.; Lin, K. J.; Du, Y. W. Synthesis, Microwave Electromagnetic, and Microwave Absorption Properties of Twin Carbon Nanocoils. *J. Phys. Chem. C* **2008**, *112*, 19316–19323.
34. Qin, Y.; Zhang, Q.; Cui, Z. L. Effect of Synthesis Method of Nanocopper Catalysts on the Morphologies of Carbon Nanofibers Prepared by Catalytic Decomposition of Acetylene. *J. Catal.* **2004**, *223*, 389–394.
35. Qin, Y.; Zhang, Z. K.; Cui, Z. L. Helical Carbon Nanofibers Prepared by Decomposition of Acetylene with a Catalyst Derived from the Decomposition of Copper Tartrate. *Carbon* **2003**, *41*, 3063–3074.
36. Qin, Y.; Zhang, Z. K.; Cui, Z. L. Helical Carbon Nanofibers with a Symmetric Growth Mode. *Carbon* **2004**, *42*, 1917–1922.
37. Zhang, Y. H.; Sun, X. Synthesis of Carbon Nanofibers and Foam by Catalytic Chemical Vapor Deposition Using a Water-Soluble Alkali Salt Catalyst. *Adv. Mater.* **2007**, *19*, 961–964.
38. Ning, Y. S.; Zhang, X. B.; Wang, Y. W.; Sun, Y. L.; Shen, L. H.; Yang, X. F.; Tendeloo, G. V. Bulk Production of Multiwall Carbon Nanotube Bundles on Sol−Gel Prepared Catalyst. *Chem. Phys. Lett.* **2002**, *366*, 555–560.
39. Dunlap, B. I. Relating Carbon Tubules. *Phys. Rev. B* **1994**, *49*, 5643–5650.
40. Dunlap, B. I. Constraints on Small Graphitic Helices. *Phys. Rev. B* **1994**, *50*, 8134–8137.
41. Terrones, H.; Terrones, M.; Hernandez, E.; Grobert, N.; Charlier, J. C.; Ajayan, P. M. New Metallic Allotropes of Planar and Tubular Carbon. *Phys. Rev. Lett.* **2000**, *84*, 1716–1719.
42. Motojima, S.; Chen, X. Q. Three-Dimensional Growth Mechanism of Cosmo-Mimetic Carbon Microcoils Obtained by Chemical Vapor Deposition. *J. Appl. Phys.* **1999**, *85*, 3919–3921.
43. Liu, Q.; Cui, Z. M.; Ma, Z.; Bian, S. W.; Song, W. Guo. Carbon Materials with Unusual Morphologies and Their Formation Mechanism. *J. Phys. Chem. C* **2007**, *111*, 12420–12424.
44. Korneva, G.; Ye, H. H.; Gogotsi, Y.; Halverson, D.; Friedman, G.; Bradley, J. C.; Kornev, K. G. Carbon Nanotubes Loaded with Magnetic Particles. *Nano Lett.* **2005**, *5*, 879–884.
45. Jang, J. S.; Yoon, H. S. Fabrication of Magnetic Carbon Nanotubes Using a Metal-Impregnated Polymer Precursor. *Adv. Mater.* **2003**, *15*, 2088–2091.
46. Xu, L. Q.; Zhang, W. Q.; Ding, Y. W.; Peng, Y. Y.; Zhang, S. Y.; Yu, W. C.; Qian, Y. T. Formation, Characterization, and Magnetic Properties of Fe_3O_4 Nanowires Encapsulated in Carbon Microtubes. *J. Phys. Chem. B* **2004**, *108*, 10859–10862.